

## Article

# Template Electrochemical Synthesis of Hydroxyapatite on a Titania–Silver Composite Surface for Potential Use in Implantology

Evgeniy V. Orekhov <sup>1</sup>, Andrey Yu. Arbenin <sup>1,\*</sup>, Elena G. Zemtsova <sup>1</sup>, Darya N. Sokolova <sup>1</sup>,  
Alexandra N. Ponomareva <sup>1</sup>, Maxim A. Shevtsov <sup>2</sup> , Natalia M. Yudintceva <sup>2</sup>  and Vladimir M. Smirnov <sup>1</sup>

<sup>1</sup> Saint Petersburg State University, 199034 Saint Petersburg, Russia; zeka333555@gmail.com (E.V.O.); ezimtsova@yandex.ru (E.G.Z.); darya.sokolova.2014@mail.ru (D.N.S.); ponomareva2710@gmail.com (A.N.P.); vms11@yandex.ru (V.M.S.)

<sup>2</sup> Institute of Cytology of the Russian Academy of Sciences (RAS), 194064 Saint Petersburg, Russia; shevtsov-max@mail.ru (M.A.S.); yudintceva@mail.ru (N.M.Y.)

\* Correspondence: aua47@yandex.ru; Tel.: +7-812-428-4033

**Abstract:** Modern materials science, both in terms of functional and structural materials, is actively developing towards the creation of structures with a given ordering. A wide range of methods involves ordering the structure according to a template shape. Template synthesis is one of the most wide-spread approaches. Most often, the template synthesis method is implemented under conditions of limiting the growth of the phase due to the geometry of the template. In the present work, a template electrochemical method is considered for calcium hydroxyapatite (HAp) coating synthesis, based on the replication of the planar template texture during deposition. In this case, the template is an array of silver microparticles immobilized on an electrically conductive substrate, separated by an insulator layer. The developed approach is similar to the mask metallization widely used in planar technology. In this work, the possibility of the template pulsed electrodeposition of ceramics rather than metal is shown using HAp as an example. This approach is interesting for materials science, in particular, for obtaining micro-ordered hydroxyapatite structures—a crystallochemical analogue of the inorganic bone tissue component—on the surface of bone implants, which can be implemented to improve their biomedical characteristics. As a result of our study, we experimentally determined the conditions for obtaining the composite coating  $\text{TiO}_2/\text{Ag}/\text{Ca}_{10}(\text{PO}_4)_6(\text{OH})_2$  with controlled phase structure, topology and localization of components on the surface, which was confirmed by Scanning Electron Microscopy, Energy Dispersive Spectroscopy, and X-ray Diffraction (SEM, EDS and XRD). The absence of cytotoxicity for the osteoblast-like cells of the developed coating was revealed by cytological tests.

**Keywords:** template electrochemical synthesis; hydroxyapatite; silver; titanium; titanium dioxide; implant



**Citation:** Orekhov, E.V.; Arbenin, A.Y.; Zemtsova, E.G.; Sokolova, D.N.; Ponomareva, A.N.; Shevtsov, M.A.; Yudintceva, N.M.; Smirnov, V.M. Template Electrochemical Synthesis of Hydroxyapatite on a Titania–Silver Composite Surface for Potential Use in Implantology. *Coatings* **2022**, *12*, 266. <https://doi.org/10.3390/coatings12020266>

Academic Editors: Noam Eliaz and Simona Liliana Iconaru

Received: 12 December 2021

Accepted: 8 February 2022

Published: 16 February 2022

**Publisher's Note:** MDPI stays neutral with regard to jurisdictional claims in published maps and institutional affiliations.



**Copyright:** © 2022 by the authors. Licensee MDPI, Basel, Switzerland. This article is an open access article distributed under the terms and conditions of the Creative Commons Attribution (CC BY) license (<https://creativecommons.org/licenses/by/4.0/>).

## 1. Introduction

Various artificial materials, such as ceramics, metals, polymers and their composites, are used to replace affected bones [1–5]. Metals and their alloys are considered to be the most suitable for replacing damaged supporting bones as compared to polymers and ceramics. Nowadays, Ti and its alloys are especially promising as biocompatible materials due to their strength and physico-chemical resistance, in combination with a relatively low price and density [6]. However, the slow osseointegration of Ti implants still remains a significant problem. To increase corrosion resistance, biocompatibility, and mechanical stability of Ti, its surface is usually modified or coated with a suitable material, while the surface nature depends on the purpose and area of implantation [7].

For bone-embedded Ti implants, the surface irregularities have a positive effect on osseointegration [8]. Tissue growth on a rough and smooth surface were compared in [9]. An uneven surface, as a rule, forms stronger contact with bone tissue, whereas a smooth surface can be encapsulated by connective tissue. This effect is due to faster osteoblast differentiation by blocking the drift along the surface with higher roughness. However, surfaces with various reliefs give different responses, which makes it impossible to unambiguously quantify the engraftability nature [10–22].

During the implantation, there is a risk of infection associated with the implant materials or bacteria ingress into the wound during surgery. The infection leads to local inflammation around the implant and, eventually, to its loss. Silver is often used as an inorganic antibacterial agent because of its broad-spectrum bactericidal properties, good biocompatibility, satisfactory safety level and inherent stability in biological fluids [23–25].

To increase the speed and improve the quality of implant engraftment, its surface is often modified with hydroxyapatite (HAp) or amorphous calcium phosphate, since HAp is one of the main components of the mineral part of the bones [26–34]. One of the most effective methods of HAp coating on the implant surface is electrochemical deposition [35–37].

In addition, a number of works describe composite coatings based on  $\text{TiO}_2/\text{Ag}/\text{HAp}$  [38–41]. These coatings have good biocompatibility and antibacterial properties. However, the methods used in published works do not produce a desired surface with a complex structure. The coating of the same type is obtained over the entire surface area. This makes these synthesis methods limited in terms of controlling the localization of the structure and composition.

In this work, we take pre-synthesized  $\text{TiO}_2/\text{Ag}$  matrix [42] with a complicated micro-level morphology as the template. We develop the technique of electrochemical HAp synthesis on the  $\text{TiO}_2/\text{Ag}$  template surface in order to create a composite  $\text{TiO}_2/\text{Ag}/\text{HAp}$  film with a controlled structure and composition: pulsed electrochemical deposition, in contrast to DC deposition, achieves the replication of the template structure by depositing hydroxyapatite. The developed synthesis approach is promising for use in bone implantation due to its ability to control the micron structure of the deposited hydroxyapatite by varying the texture of the initial template and composition of the composite coating that combines a two-level relief hierarchy [43–45] formed by xerogel globules and micron electrochemical deposit and the presence of HAp and silver.

## 2. Materials and Methods

### 2.1. Fabrication of the Initial $\text{TiO}_2$ Film Matrix

Initially, Ti substrates were coated with textured  $\text{TiO}_2$  to obtain a template by modifying the sol–gel method developed by us [46]. Nanosilica-polished (Mastermet, Buehler, Lake Bluff, IL, USA) technical Ti VT1-0 (VSMPO-AVISMA Corporation, Verkhnyaya Salda, Russia) with a size of 10 mm × 38 mm with rounded edges was used as a substrate. The roughness was <0.01  $\mu\text{m}$ . For the film synthesis, we used an absolute isopropanol (iPA, Vecton, Saint-Petersburg, Russia), titanium tetraisopropoxide (TTIP, Sigma Aldrich, Saint Louis, MO, USA), diethanolamine (DEA, Sigma Aldrich, Saint Louis, MO, USA) and polyethylene glycol Mw = 20,000 D (PEG, Merck, Darmstadt, Germany) in the ratio iPA/TTIP/DEA/ $\text{H}_2\text{O}$ /PEG = 773/227/105/36/29. Before applying the coating, the solution was preheated to 45 °C with stirring to dissolve the PEG. The film was obtained by the sol–gel method with dip coating using equipment KSV Nima Dip Coater, Singlevessel (KSV Nima, Espoo, Finland). The extraction rate was 100 mm/min. Then, the deposited film was subjected to heat treatment (hot plate: 5 min, 400 °C), which led to pore formation and partial cracking. After that, the  $\text{TiO}_2$  film was treated with boiling deionized water and dried in air at 200 °C to remove excess moisture.

## 2.2. Electrochemical Silver Deposition

An aqueous electrolyte of the following composition was used to precipitate silver: AgNO<sub>3</sub> (Vecton, Saint-Petersburg, Russia)—3.15 g; sulfosalicylic acid (Vecton, Russia)—11 g with a 25% aqueous ammonia addition (Vecton, Russia) until reaching pH = 9. The resulting solution was diluted to 100 mL with deionized water. A potentiostat-galvanostat Elins P45X (Chernogolovka, Russia) was used for the template deposition. Silver was deposited in a polypropylene cell with stirring, where a Ti substrate coated with a perforated TiO<sub>2</sub> xerogel film was used as a working electrode, and Ag electrode was used as a counter electrode. The pulse mode for synthesis included 750 cycles with the sequence: 1 V—5 ms; 0.3 V—3 ms; 2 V—10 ms; and 0 V—65 ms.

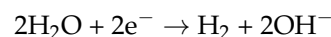
## 2.3. Electrochemical HAp Deposition

Coatings of calcium phosphate structures, including HAp, were obtained on an Ellins P45X (Chernogolovka, Russia) potentiostat-galvanostat by electrochemical template synthesis using TiO<sub>2</sub>/Ag composite as the cathode and template, and graphite as the anode. Based on the HAp ratio Ca/P = 1.67, we used 1.18 g of calcium nitrate (Ca(NO<sub>3</sub>)<sub>2</sub>, Vecton, Saint-Petersburg, Russia) and 0.411 g of potassium dihydrophosphate (KH<sub>2</sub>PO<sub>4</sub>, Vecton, Russia) per 100 mL of deionized water. Depending on the sample, HAp precipitated either at a constant or at a pulsed current.

During synthesis, the following reactions occur:

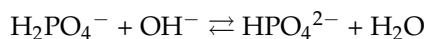
On the cathode:

- (1) electrochemical water splitting



In the near-cathode area:

- (2) hydroxide ions react with dihydrophosphate ions

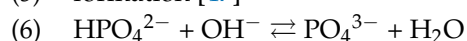


- (3) Ca<sup>2+</sup> combined with HPO<sub>4</sub><sup>2-</sup>, CaHPO<sub>4</sub>·2H<sub>2</sub>O deposited on the electrode



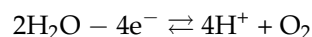
- (4) at a high OH<sup>-</sup> concentration, reactions lead to the HAp

- (5) formation [47]

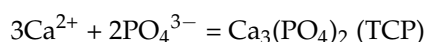
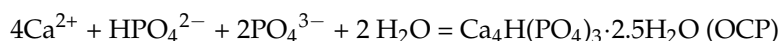


On the anode:

- (8) electrochemical water splitting



In addition to the described processes, the precipitation of tricalcium phosphate (TCP) and octacalcium phosphate (OCP) is possible [48]



After deposition, the coated substrate was washed with distilled water and air dried.

#### 2.4. Sample Characteristics

The structure and morphology of the coatings were studied using a scanning electron microscope Merlin (Carl Zeiss Microscopy GmbH, Jena, Germany); for microanalysis and the construction of element maps, we used the EDS console (Oxford Instruments INCAx-act, Abingdon, UK) for a scanning microscope Zeiss Merlin. The Rigaku “MiniFlex II” (Tokyo, Japan) X-ray diffractometer was used for X-ray phase analysis. X-rays with a wavelength of 1.5406 Å were used for the analysis.

Cytotoxicity studies were performed employing osteoblast precursor cell line MG-63 obtained from the shared research facility “Vertebrate cell culture collection” of the Institute of Cytology of the Russian Academy of Sciences (Saint Petersburg, Russia). Cells were grown in minimum essential medium (MEM, Gibco, Waltham, MA, USA) supplemented with 10% fetal bovine serum (FBS, Thermo Fisher Scientific, Carlsbad, CA, USA) and 50 µg/mL gentamicin (Gibco, Carlsbad, CA, USA) at 37 °C and 5% CO<sub>2</sub>. The cells viability on the surfaces of samples was assessed using the MTT (3-(4,5-dimethylthiazol-2-yl)-2,5-diphenyltetrazolium bromide) test [49]. Cells were incubated for 1, 6, 12, 24, and 48 h in a CO<sub>2</sub> incubator on the surface of samples. Following co-incubation, the cells’ proliferative activity was assessed employing Vybrant™ MTT Cell Proliferation Assay Kit according to the manufacturer’s protocol (Invitrogen, Waltham, MA, USA). Proliferation was quantified by measuring optical absorbance at 570 nm on a Bio-Rad 680 microplate photometer (Bio-Rad LABORATORIES, Hercules, CA, USA). Each experimental series contained 5 samples. Initially, the arithmetic mean and standard deviation were calculated. Half the width of the confidence range was the quantile of the Student’s t-distribution ( $p = 0.95$ ) multiplied by the standard deviation divided by the square root of the number of repetitions of measurements (5 times).

### 3. Results and Discussion

#### 3.1. X-ray Diffraction (XRD) Determination of the Phase Composition of Electrochemically Deposited Calcium Phosphates

As a result of the XRD study of the samples obtained by electrochemical deposition at direct current at different potentials, the correlation of the phase composition with the conditions of electrochemical deposition was revealed (Figure 1). The values of 35.08° (1,0,0), 38.43° (0,0,2), 40.16° (1,0,1), 53.00° (1,0,2), 62.93° (1,1,0), 70.67° (1,0,3), 76.20° (1,1,2), 77.33° (2,0,1), 82.32° (0,0,4), 86.74° (2,0,2), 92.75° (1,0,4) originate from the substrate (this set is typical for metallic Ti JCPDS No. 44-1294). The peaks corresponding to the electrochemical deposit vary with the potential growth.

Separately, to identify the phase composition changes of electrochemically deposited calcium phosphates, an area containing characteristic peaks of Hap—JCPDS No. 9-0432 (25.88° (0,0,2), 31.77° (1,2,1), 32.20° (1,1,2), 32.91° (0,3,0)) and monetite—JCPDS No. 70-360 (26.36° (0,0,2), 26.55° (2,0,0), 26.69° (−2,0,1), 30.24° (−1,2,0), 32.35° (1,0,2), 32.46° (2,0,1), 32.83° (−2,0,2), 32.97° (−1,2,1)) was constructed (Figure 2). Based on the change in the peaks’ height, we established the potential dependence of the phase composition. At 3.0, 3.5 V, we observe mainly the monetite phase; at potentials of 4.0, 4.25, 4.5 V, both phases are present, whereas at 4.75 V and higher, the HAp phase is preferable.

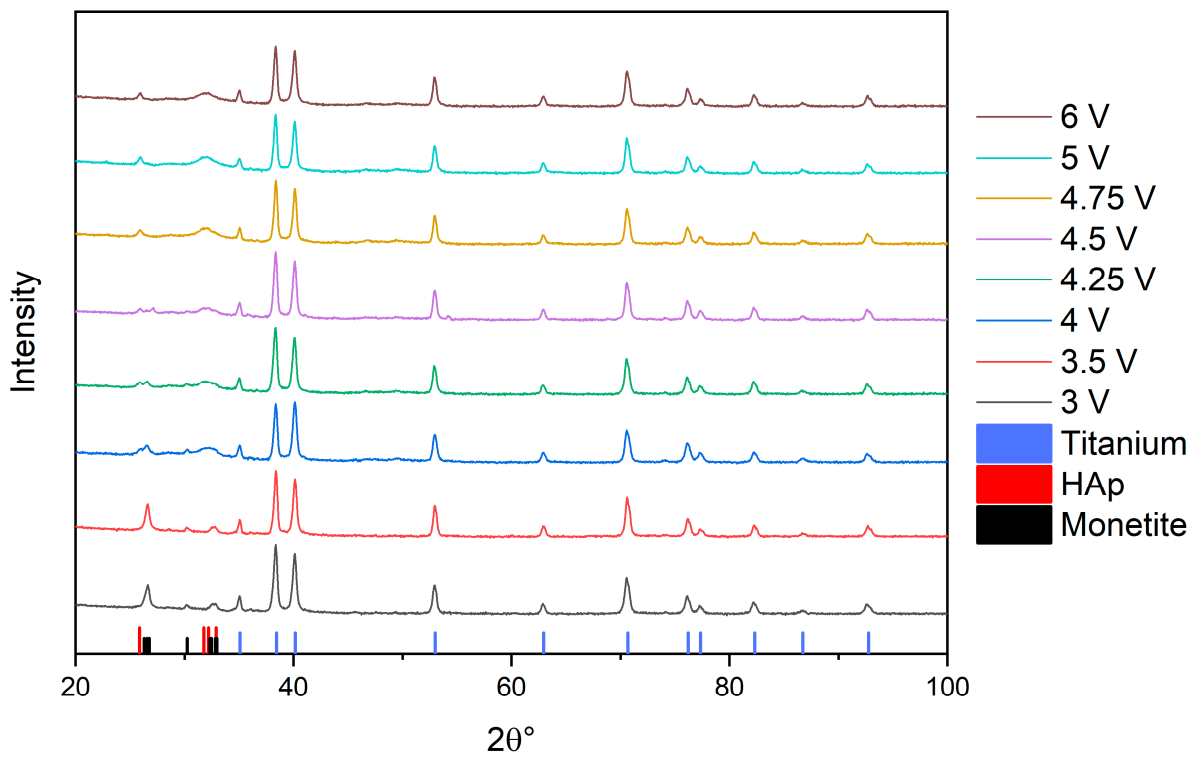


Figure 1. XRD patterns of calcium phosphate phase distributions.

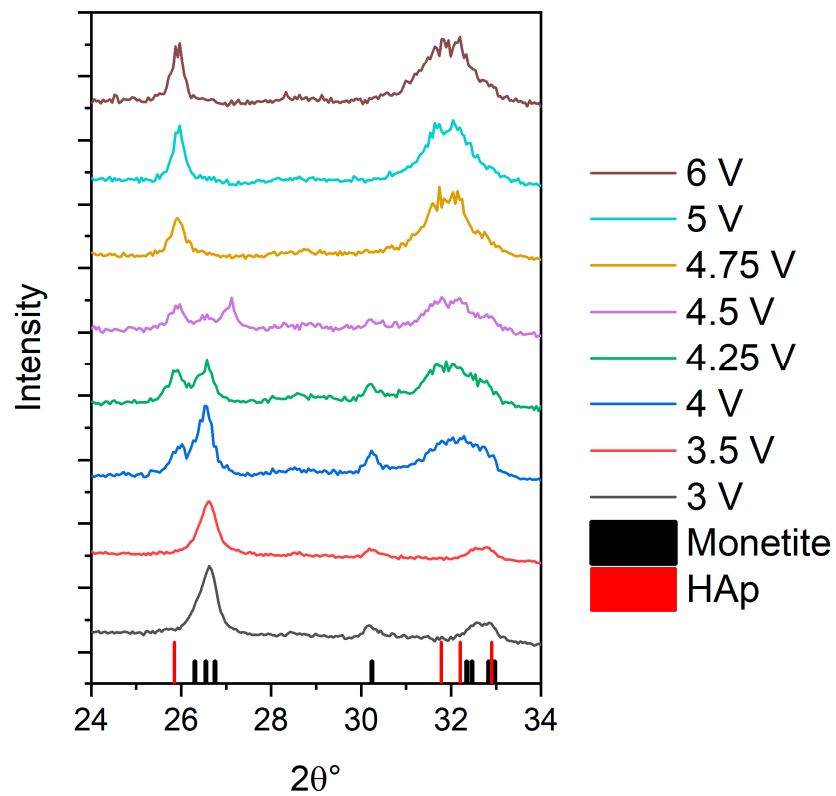


Figure 2. Dynamics of the transformation of monetite and hydroxyapatite peaks during the increase in potential.

### 3.2. Investigation of the Structure and Elemental Composition of the TiO<sub>2</sub>/Ag/HAp Composite Coating by Scanning Electron Microscopy (SEM) and Energy Dispersive Spectroscopy (EDS)

A series of experiments for the HAp synthesis by template electrochemical deposition under constant and pulsed currents was carried out. The conditions were chosen based on XRD of HAp samples deposited at different potentials (low deposition potentials were excluded to avoid the monetite formation (Table 1))

**Table 1.** Conditions for the HAp synthesis.

Sample No.	Deposition Mode			
1	Constant Current	6 V ( $\tau = 15$ min)		
2	1200 cycles	12 V $\tau = 3$ ms	−2 V $\tau = 2$ ms	0 V $\tau = 85$ ms

A micrograph of the initial Ti/TiO<sub>2</sub>/Ag composite is shown in Figure 3 for comparison. The structure of this template is very complex, so the spontaneous deposition of hydroxyapatite replicating the pattern of silver star-shaped particles is impossible. This makes this template convenient for estimating the efficiency of the conditions for template electrochemical synthesis.

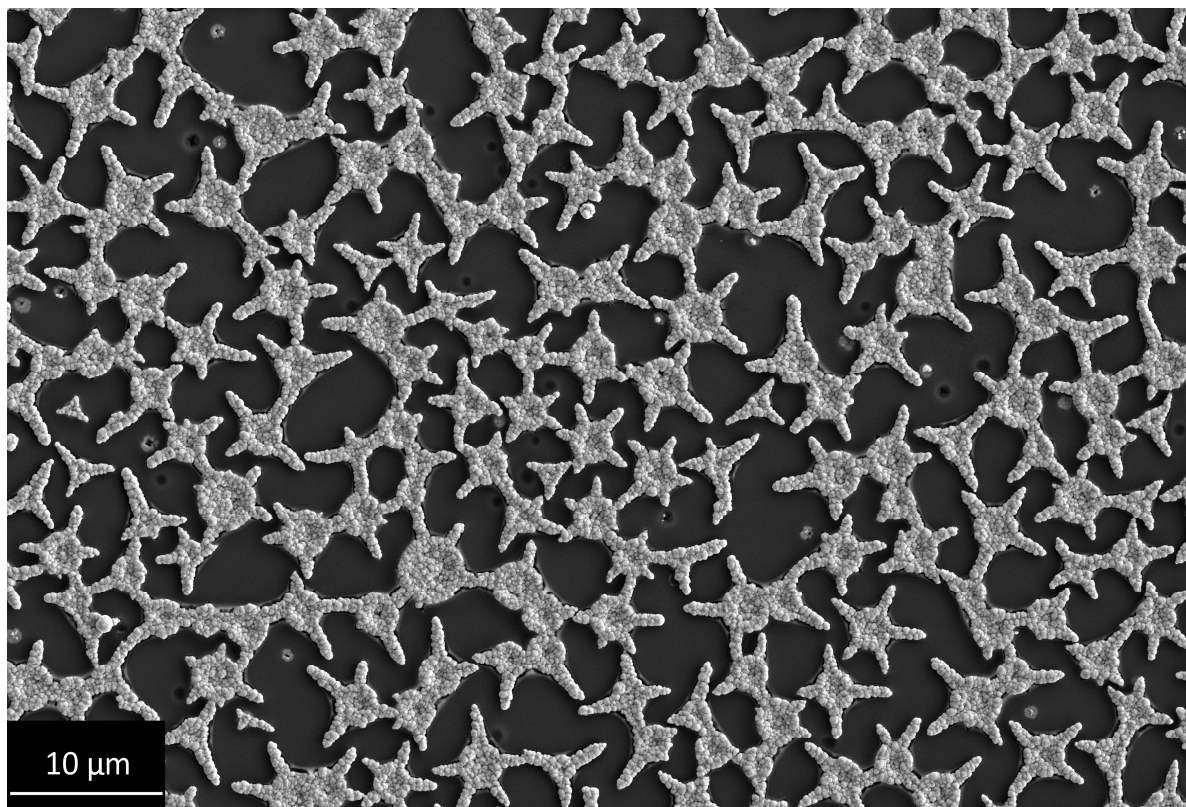


**Figure 3.** Micrograph of the initial Ti/TiO<sub>2</sub>/Ag composite.

The micrograph of sample 1 Figure 4 shows the formation of calcium phosphate structures; this is also confirmed by the Ca and P elemental maps Figure 5. However, the micrograph and elemental maps showed the absence of template deposition: the cracked layer of hydroxyapatite covered the entire surface of the sample. This can be explained by the HAp formation mechanism: electrochemically generated hydroxide ions intensively migrate from the silver/electrolyte interface. In this case, all areas of the composite surface can be coated with HAp.

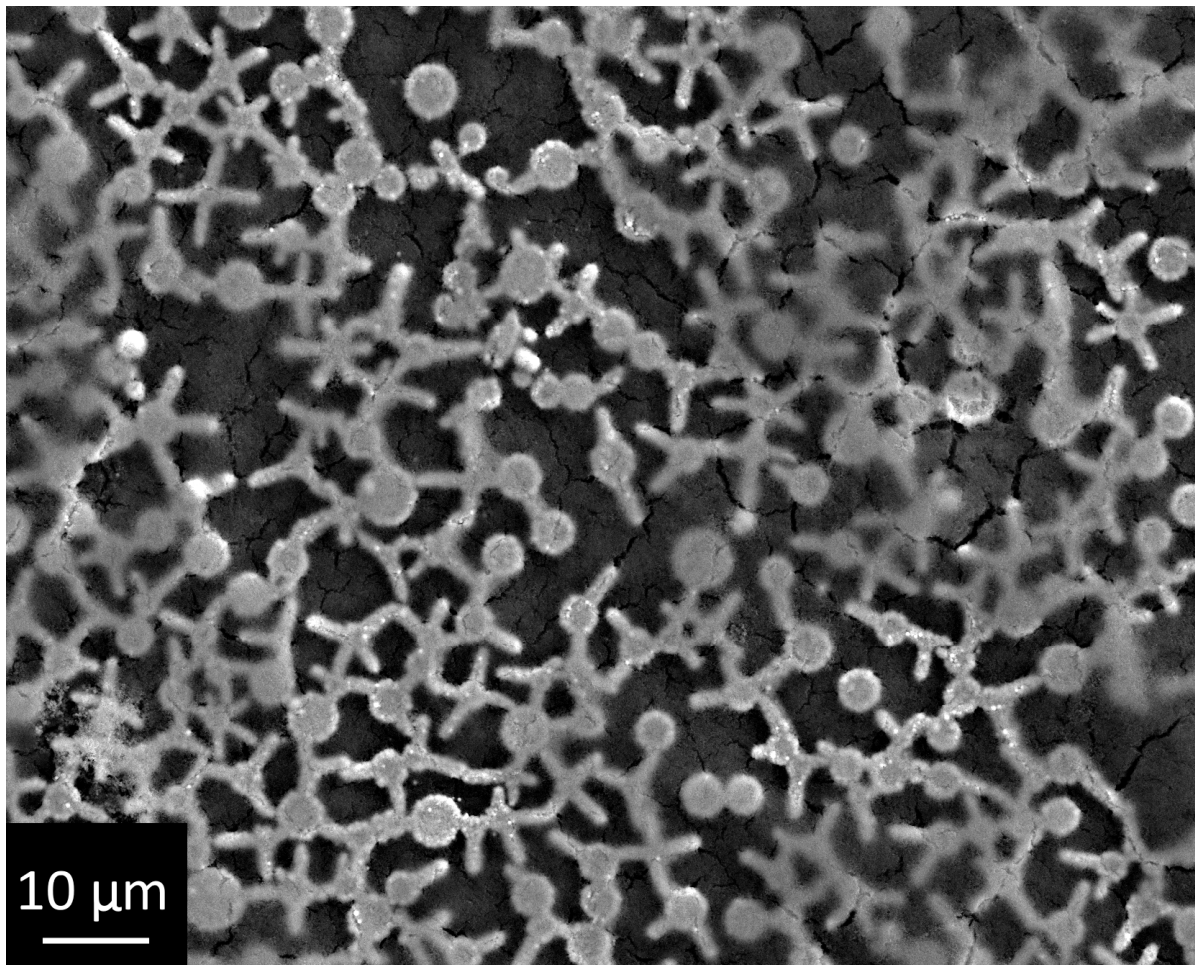


**Figure 4.** Micrograph of the sample with constant current deposited HAp.

By analogy with the electrochemical Ag deposition, it was supposed that the cyclic mode could improve the coating quality. The assumption was based on the fact, that in short pulses at high currents around the Ag microelectrodes, there would be a region with a high pH value, in which HAp deposition would proceed rapidly. In this case, it was assumed that it would be possible to precipitate HAp according to the template texture.

Pulsed deposition provides a structure without a continuous HAp layer on the sample surface (Figure 6).

The deposited HAp replicates the template geometry, although it is clear from the Ca and P elemental maps that HAp is still spread over the coating surface outside the silver-covered areas (Figure 7). As the recent review of the topic of hydroxyapatite electrodeposition shows [50], this direction is relevant despite decades of active research: the study of the influence of deposition conditions on the properties of the deposit is actively developing. However, the results presented show that, in contrast to the existing methods of deposit formation with a given morphology, phase composition, and chemical composition, it becomes possible due to the use of template to deposit hydroxyapatite-based coatings with a given micron structure.

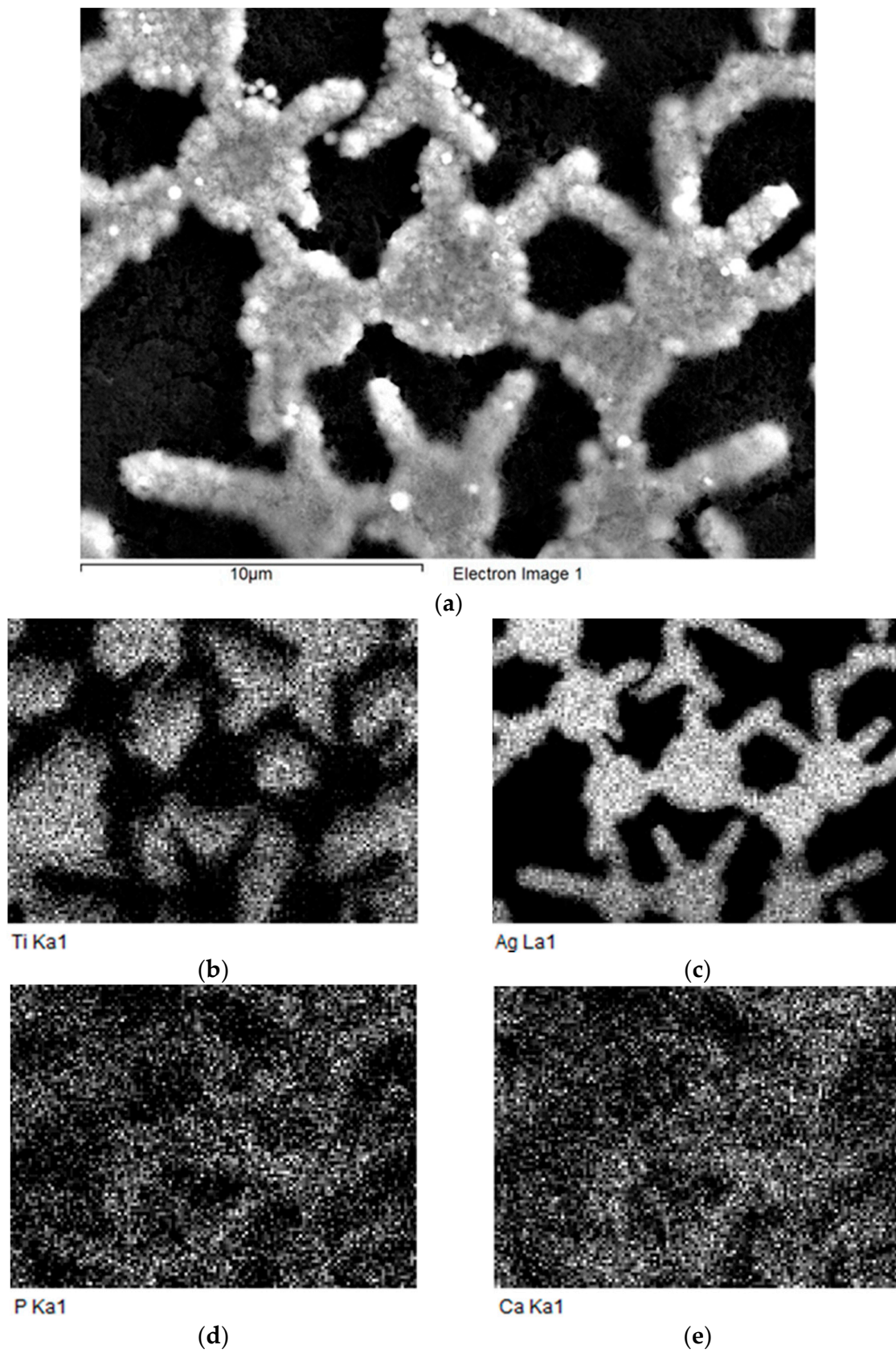


**Figure 5.** Elemental maps of the sample 1 with constant current deposited HAp. (a)—scanning electron micrography, elemental maps: (b)—Ti, (c)—Ag, (d)—P, (e)—Ca.

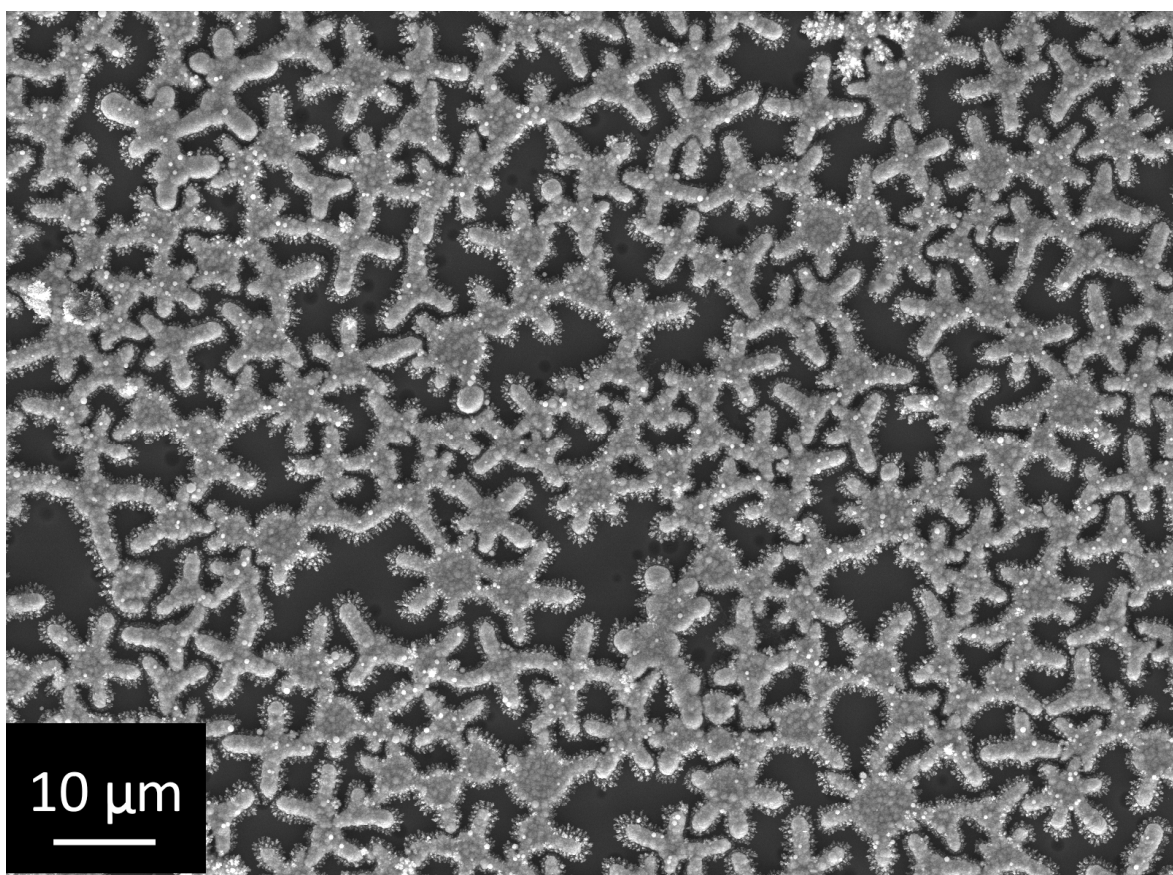


**Figure 6.** Micrograph of the sample with pulsed current deposited HAp.

XRD proved the crystal structure of our deposited film (Figure 8). In this diffractogram peaks correspond to substrate (Ti), silver (Ag—JCPDS No. 04-0783; silver microparticles that form template structure) and HAp. Similar results were obtained in the article [51]: the authors carried out pulsed the electrochemical deposition of cobalt-doped hydroxyapatite on a titanium substrate from an electrolyte based on calcium nitrate and ammonium dihydrophosphate. As in our case, XRD showed the presence of the hydroxyapatite phase.

In next stage of that sample analysis, comparative cytological studies were performed. The results of the proliferative activity assessment of MG-63 cells cultured on the surface of pure Ti, Ti coated with a perforated TiO<sub>2</sub> xerogel film, Ti coated with a perforated TiO<sub>2</sub> xerogel with Ag deposited in the perforation and sample 2 (Ti/TiO<sub>2</sub>/Ag/Ca<sub>10</sub>(PO<sub>4</sub>)<sub>6</sub>(OH)<sub>2</sub>) are shown in Figure 9. On the basis of the obtained data, it can be concluded that, when cells were grown on the surface of all the studied samples, their viability does not differ from the control during the entirety of the co-incubation period (48 h).

The ultrastructural organization of MG-63 indicates that the cells have normal functional activity (Figure 10).

The nucleus occupies a significant part of the cell volume and has an elongated shape. As a rule, the nucleus contains a single nucleolus of the nucleolonema type, up to 0.1 μm in diameter. The nucleoplasm also contains electron-dense perichromatin granules (Figure 10A). The cytoplasm contains a well-developed protein synthesis system. The entire volume of the cytoplasm is filled with free ribosomes, short mitochondria (mi), numerous vacuoles (about 0.2 μm) with electron-transparent content (v) and cisternae of rough endoplasmic reticulum, which form an extensive network of expanded channels (ca) (Figure 10B,C). All the tested samples, including the sample with the composite coating developed in this study, do not exhibit toxicity towards MG-63 cells.

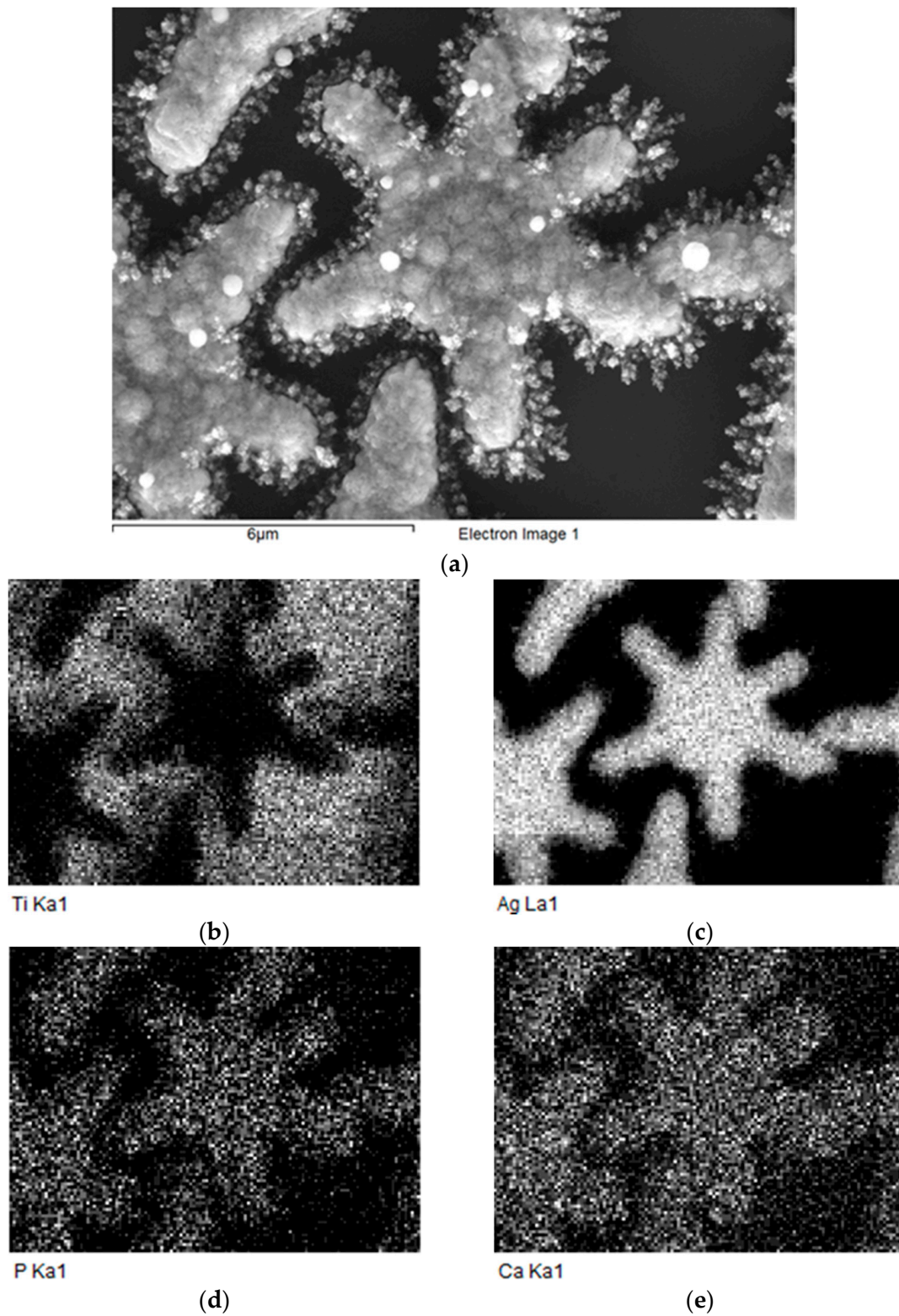


**Figure 7.** Elemental maps of the sample 2 with pulsed current deposited HAp. (a)—scanning electron micrography, elemental maps: (b)—Ti, (c)—Ag, (d)—P, (e)—Ca.

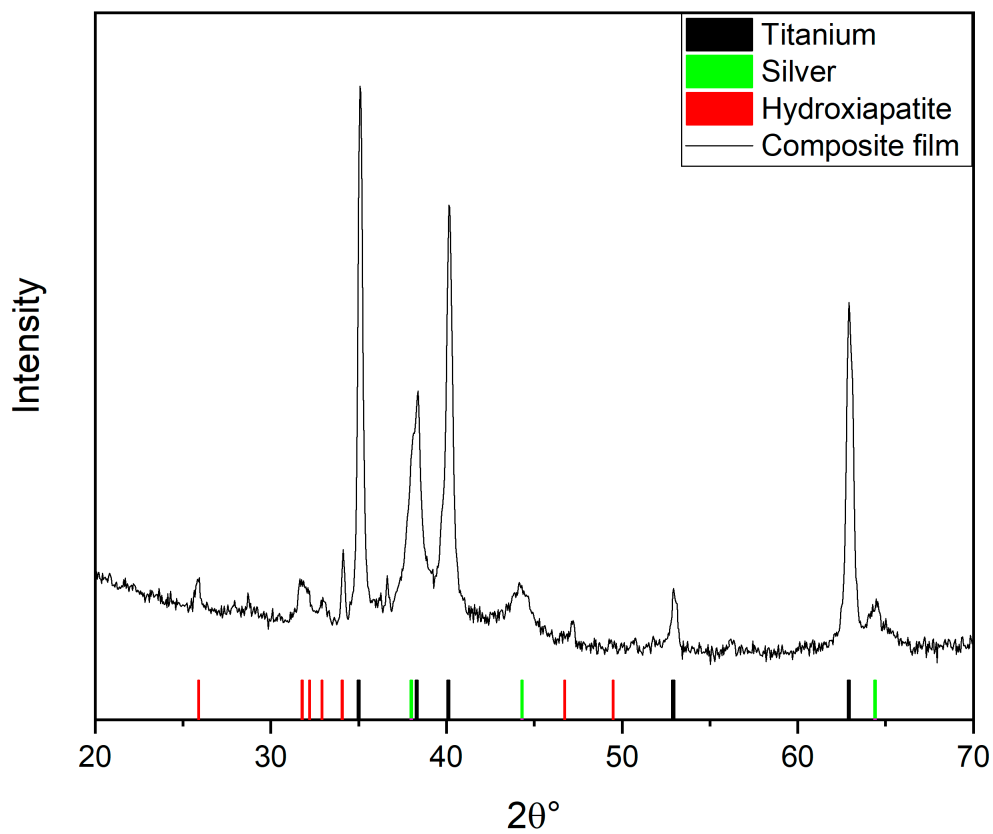


Figure 8. XRD of the sample with pulsed current deposited HAp.

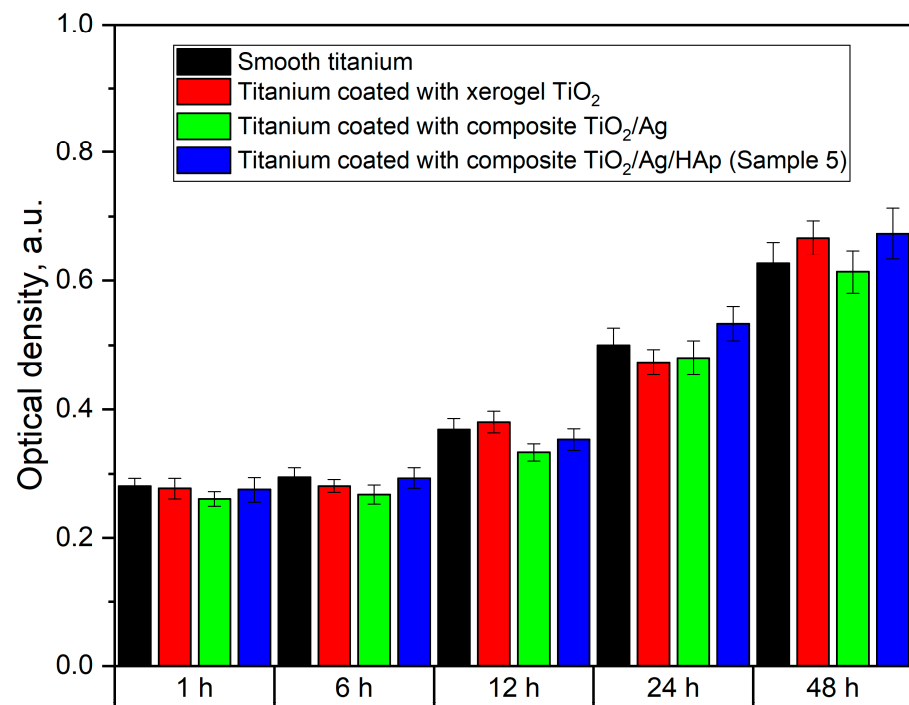
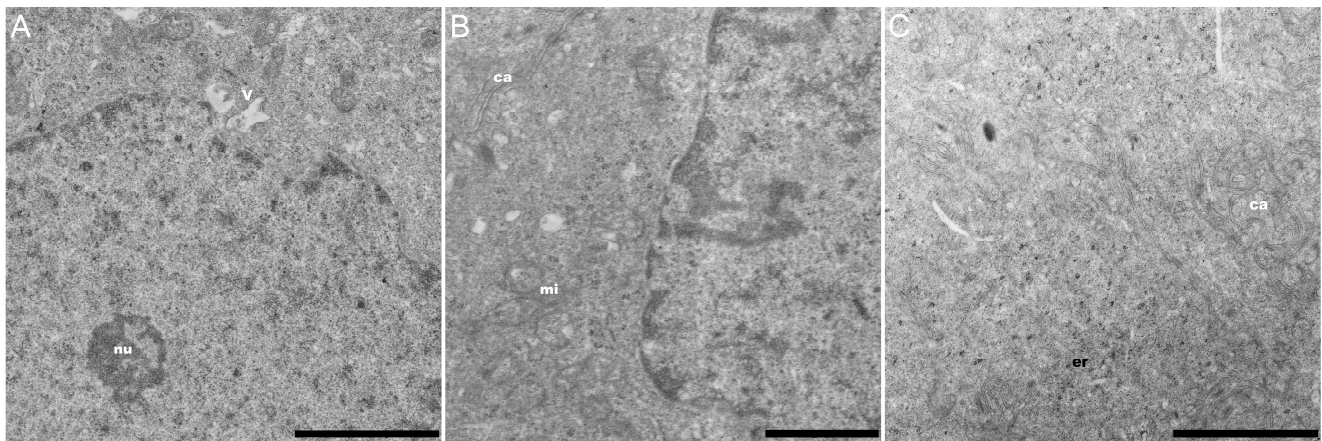


Figure 9. Proliferation activity of MG-63 cells on the sample surface with pulsed current deposited HAp.



**Figure 10.** Electron microscopy image. Ultrathin section of cultured MG-63. (A) The nucleoplasm with vacuoles and electron-dense perichromatin granules. (B) The cytoplasm with mitochondria and channels. (C) The cytoplasm with cisternae of rough endoplasmic reticulum (rER), which form channels. Scale bars (A,C): 2  $\mu\text{m}$ ; (B): 1  $\mu\text{m}$ . nu, nucleus; mi, mitochondria; v, vacuoles; ca, channels.

#### 4. Conclusions

As a result of this work, a method was developed that allows the template electrochemical synthesis of hydroxyapatite. The obtained hydroxyapatite is deposited in the form of micron objects, which replicate the original template topology. It is also shown that electro-chemical deposit is not cytotoxic for osteoblast-like cells. The developed method can be of interest for developing coatings for bone implantation, because, in contrast to conventional electrochemical deposition, it becomes possible to create a hydroxyapatite-based coating with the topology required by the researcher.

**Author Contributions:** conceptualization, E.V.O. and A.Y.A.; methodology, D.N.S. and A.N.P.; cytology analysis, M.A.S. and N.M.Y.; investigation, E.V.O., V.M.S., and A.Y.A.; writing—original draft preparation, E.V.O. and A.Y.A.; writing—review and editing, E.G.Z.; All authors have read and agreed to the published version of the manuscript.

**Funding:** The study was supported by St. Petersburg State University (ID: 74883303).

**Institutional Review Board Statement:** Not applicable.

**Informed Consent Statement:** Not applicable.

**Data Availability Statement:** Data sharing is not applicable to this article.

**Acknowledgments:** The research was carried out using the equipment of the resource centers of the St. Petersburg State University Scientific Park “X-ray Diffraction research methods”, “Centre for Innovative Technologies of Composite Nanomaterials” and “Nanotechnology”.

**Conflicts of Interest:** The authors declare no conflict of interest.

#### References

1. Greenspan, D.C. Bioactive ceramic implant materials. *Current Opinion in Solid State and Materials*. *Science* **1999**, *4*, 389–393.
2. Niinomi, M.; Nakai, M.; Hieda, J. Development of new metallic alloys for biomedical applications. *Acta Biomater.* **2012**, *8*, 3888–3903. [[PubMed](#)]
3. Liang, S.X.; Feng, X.J.; Yin, L.X.; Liu, X.Y.; Ma, M.Z.; Liu, R.P. Development of a new  $\beta$  Ti alloy with low modulus and favorable plasticity for implant material. *Mater. Sci. Eng. C* **2016**, *61*, 338–343. [[CrossRef](#)] [[PubMed](#)]
4. Hussain, M.; Naqvi, R.A.; Abbas, N.; Khan, S.M.; Nawaz, S.; Hussain, A.; Zahra, N.; Khalid, M.W. Ultra-High-Molecular-Weight-Polyethylene (UHMWPE) as a Promising Polymer Material for Biomedical Applications: A Concise Review. *Polymers* **2020**, *12*, 323.
5. Zhukova, P.A.; Senatov, F.S.; Zadorozhnyy, M.Y.; Chmelyuk, N.S.; Zaharova, V.A. Polymer Composite Materials Based on Polylactide with a Shape Memory Effect for “Self-Fitting” Bone Implants. *Polymers* **2021**, *13*, 2367. [[CrossRef](#)] [[PubMed](#)]

6. Shevtsov, M.; Gavrilov, D.; Yudintceva, N.; Zemtsov, E.; Arbenin, A.; Smirnov, V.; Voronkina, I.; Adamova, P.; Blinova, M.; Mikhailova, N.; et al. Protecting the skin-implant interface with transcutaneous silver-coated skin-and-bone-integrated pylon in pig and rabbit dorsum models. *J. Biomed. Mater. Res.-Part B Appl. Biomater.* **2021**, *109*, 584–595. [[CrossRef](#)] [[PubMed](#)]
7. Williams, D.F. *Titanium for Medical Applications. Titanium in Medicine*; Springer: Berlin/Heidelberg, Germany, 2001; pp. 13–24.
8. Wennerberg, A.; Albrektsson, T.; Andersson, B.; Krol, J.J. A histomorphometric study of screw-shaped and removal torque titanium implants with three different surface topographies. *Clin. Oral Implants. Res.* **1995**, *6*, 24–30. [[CrossRef](#)] [[PubMed](#)]
9. Schmidt, C.; Kaspar, D.; Sarkar, M.R.; Claes, L.E.; Ignatius, A.A. A scanning electron microscopy study of human osteoblast morphology on five orthopedic metals. *J. Biomed. Mater. Res. Part A* **2002**, *63*, 252–261. [[CrossRef](#)] [[PubMed](#)]
10. Yang, F.; Dong, W.J.; He, F.M.; Wang, X.X.; Zhao, S.F.; Yang, G.L. Osteoblast response to porous titanium surfaces coated with zinc-substituted hydroxyapatite. *Oral Surg. Oral Med. Oral Pathol. Oral Radiol.* **2012**, *113*, 313–318. [[CrossRef](#)]
11. Zhu, X.; Son, D.W.; Ong, J.L.; Kim, K. Characterization of hydrothermally treated anodic oxides containing Ca and P on titanium. *J. Mater. Sci. Mater. Med.* **2003**, *14*, 629–634. [[CrossRef](#)]
12. Roy, M.; Bandyopadhyay, A.; Bose, S. Induction plasma sprayed nano hydroxyapatite coatings on titanium for orthopaedic and dental implants. *Surf. Coat. Technol.* **2011**, *205*, 2785–2792. [[CrossRef](#)] [[PubMed](#)]
13. Keller, J.C.; Stanford, C.M.; Wightman, J.P.; Draughn, R.A.; Zaharias, R. Characterizations of titanium implant surfaces. *J. Biomed. Mater. Res. Part A* **1994**, *28*, 939–946. [[CrossRef](#)] [[PubMed](#)]
14. Bucci-Sabattini, V.; Cassinelli, C.; Coelho, P.G.; Minnici, A.; Trani, A.; Ehrenfest, D.M.D. Effect of titanium implant surface nanoroughness and calcium phosphate low impregnation on bone cell activity in vitro. *Oral Surg. Oral Med. Oral Pathol. Oral Radiol. Endod.* **2010**, *109*, 217–224. [[PubMed](#)]
15. Juodzbalsys, G.; Sapragniene, M.; Wennerberg, A.; Baltrukonis, T. Titanium dental implant surface micromorphology optimization. *J. Oral Implantol.* **2007**, *33*, 177–185. [[CrossRef](#)]
16. Zemtsova, E.G.; Yudintceva, N.M.; Morozov, P.E.; Valiev, R.Z.; Smirnov, V.M.; Shevtsov, M.A. Improved osseointegration properties of hierarchical microtopographic/nanotopographic coatings fabricated on titanium implants. *Int. J. Nanomed.* **2018**, *13*, 2175–2188. [[CrossRef](#)] [[PubMed](#)]
17. Zemtsova, E.G.; Arbenin, A.Y.; Yudintceva, N.M.; Valiev, R.Z.; Orekhov, E.V.; Smirnov, V.M. Bioactive coating with two-layer hierarchy of relief obtained by sol-gel method with shock drying and osteoblast response of its structure. *Nanomaterials* **2010**, *7*, 323. [[CrossRef](#)] [[PubMed](#)]
18. Vetrone, F.; Variola, F.; Tambasco, P.; Zalzal, S.F.; Yi, J.H.; Sam, J.; Nanci, A. Nanoscale Oxidative Patterning of Metallic Surfaces to Modulate Cell Activity and Fate. *Nano Lett.* **2009**, *9*, 659–665. [[CrossRef](#)] [[PubMed](#)]
19. Yeniyol, S.; Bölükbaşı, N.; Çakir, A.F.; Bilir, A.; Özdemir, T. Effects of surface modifications with oxalic acid etching and sandblasting on surface topography and biocompatibility of cpTi surfaces. *Biotechnol. Biotechnol. Equip.* **2013**, *27*, 3995–4001. [[CrossRef](#)]
20. Goudarzi, M.; Batmanghelich, F.; Afshar, A.; Dolati, A.; Mortazavi, G. Development of electrophoretically deposited hydroxyapatite coatings on anodized nanotubular TiO<sub>2</sub> structures: Corrosion and sintering temperature. *Appl. Surf. Sci.* **2014**, *301*, 250–257. [[CrossRef](#)]
21. Catauro, M.; Papale, F.; Bollino, F. Characterization and biological properties of TiO<sub>2</sub>/PCL hybrid layers prepared via sol-gel dip coating for surface modification of titanium implants. *J. Non-Cryst. Solids* **2015**, *415*, 9–15. [[CrossRef](#)]
22. Kajihara, K.; Nakanishi, K.; Tanaka, K.; Hirao, K.; Soga, N. Preparation of Macroporous Titania Films by a Sol-Gel Dip-Coating Method from the System Containing Poly (ethylene glycol). *J. Am. Ceram. Soc.* **1998**, *81*, 2670–2676. [[CrossRef](#)]
23. Tian, B.; Chen, W.; Yu, D.; Lei, Y.; Ke, Q.; Guo, Y.; Zhu, Z. Fabrication of silver nanoparticle-doped hydroxyapatite coatings with oriented block arrays for enhancing bactericidal effect and osteoinductivity. *J. Mech. Behav. Biomed. Mater.* **2016**, *6*, 345–359. [[CrossRef](#)] [[PubMed](#)]
24. Mai, L.; Wang, D.; Zhang, S.; Xie, Y.; Huang, C.; Zhang, Z. Synthesis and bactericidal ability of Ag/TiO<sub>2</sub> composite films deposited on titanium plate. *Appl. Surf. Sci.* **2010**, *257*, 974–978. [[CrossRef](#)]
25. Yu, B.; Leung, K.M.; Guo, Q.; Lau, W.M.; Yang, J. Synthesis of Ag–TiO<sub>2</sub> composite nano thin film for antimicrobial application. *Nanotechnology* **2011**, *22*, 115603. [[CrossRef](#)]
26. Arbenin, A.Y.; Zemtsova, E.G.; Orekhov, E.V.; Smirnov, V.M. Features of the sol-gel synthesis of TiO<sub>2</sub> nanolayers with calcium phosphate structures on titanium surface. *Russ. J. Gen. Chem.* **2017**, *87*, 340–341. [[CrossRef](#)]
27. Fu, C. *Synthesis and Characterization of Hydroxyapatite Coatings for Medical Applications*; University of Rochester: Rochester, NY, USA, 2016; pp. 46–70.
28. Buser, D.; Schenk, R.K.; Steinemann, S.; Fiorellini, J.P.; Fox, C.H.; Stich, H. Influence of surface characteristics on bone integration of titanium implants. A histomorphometric study in miniature pigs. *J. Biomed. Mater. Res. Part A* **1991**, *25*, 889–902. [[CrossRef](#)]
29. Li, T.; Lee, J.; Kobayashi, T.; Aoki, H. Hydroxyapatite coating by dipping method, and bone bonding strength. *J. Mater. Sci. Mater. Med.* **1996**, *7*, 355–357. [[CrossRef](#)]
30. Yang, G.L.; He, F.M.; Hu, J.A.; Wang, X.X.; Zhao, S.F. Biomechanical comparison of biomimetically and electrochemically deposited hydroxyapatite-coated porous titanium implants. *J. Oral Maxillofac. Surg.* **2010**, *68*, 420–427. [[PubMed](#)]
31. Webster, T.J.; Ergun, C.; Doremus, R.H.; Siegel, R.W.; Bizios, R. Enhanced functions of osteoblasts on nanophase ceramics. *Biomaterials* **2000**, *21*, 1803–1810. [[CrossRef](#)]

32. Shi, Z.; Huang, X.; Cai, Y.; Tang, R.; Yang, D. Size effect of hydroxyapatite nanoparticles on proliferation and apoptosis of osteoblast-like cells. *Acta Biomater.* **2009**, *5*, 338–345. [[CrossRef](#)] [[PubMed](#)]
33. Werner, J.; Linner-Krčmar, B.; Friess, W.; Greil, P. Mechanical properties and in vitro cell compatibility of hydroxyapatite ceramics with graded pore structure. *Biomaterials* **2002**, *23*, 4285–4294. [[CrossRef](#)]
34. Wenisch, S.; Stahl, J.P.; Horas, U.; Heiss, C.; Kilian, O.; Trinkaus, K.; Hild, A.; Schnettler, R. In vivo mechanisms of hydroxyapatite ceramic degradation by osteoclasts: Fine structural microscopy. *J. Biomed. Mater. Res. Part A* **2003**, *67*, 713–718. [[CrossRef](#)]
35. Thanh, D.T.M.; Nam, P.T.; Phuong, N.T.; Van Anh, N.; Hoang, T.; Dai Lam, T. Controlling the electrodeposition, morphology and structure of hydroxyapatite coating on 316L stainless steel. *Mater. Sci. Eng. C* **2013**, *33*, 2037–2045. [[CrossRef](#)] [[PubMed](#)]
36. Kuo, M.C.; Yen, S.K. The process of electrochemical deposited hydroxyapatite coatings on biomedical titanium at room temperature. *Mater. Sci. Eng. C* **2002**, *20*, 153–160. [[CrossRef](#)]
37. Eliaz, N.S.T.M.; Sridhar, T.M.; Kamachi Mudali, U.; Raj, B. Electrochemical and electrophoretic deposition of hydroxyapatite for orthopaedic applications. *Surf. Eng.* **2005**, *21*, 238–242. [[CrossRef](#)]
38. Lu, X.; Zhang, B.; Wang, Y.; Zhou, X.; Weng, J.; Qu, S.; Feng, B.; Watari, F.; Ding, Y.; Leng, Y. Nano-Ag-loaded hydroxyapatite coatings on titanium surfaces by electrochemical deposition. *J. R. Soc. Interface* **2011**, *8*, 529–539. [[CrossRef](#)]
39. Reddy, P.M.; Venugopal, A.; Subrahmanyam, M. Hydroxyapatite-supported Ag–TiO<sub>2</sub> as Escherichia coli disinfection photocatalyst. *Water Res.* **2007**, *41*, 379–386. [[CrossRef](#)] [[PubMed](#)]
40. Yan, Y.; Zhang, X.; Huang, Y.; Ding, Q.; Pang, X. Antibacterial and bioactivity of silver substituted hydroxyapatite/TiO<sub>2</sub> nanotube composite coatings on titanium. *Appl. Surf. Sci.* **2014**, *314*, 348–357. [[CrossRef](#)]
41. Mo, A.; Liao, J.; Xu, W.; Xian, S.; Li, Y.; Bai, S. Preparation and antibacterial effect of silver–hydroxyapatite/titania nanocomposite thin film on titanium. *Appl. Surf. Sci.* **2008**, *255*, 435–438. [[CrossRef](#)]
42. Arbenin, A.; Zemtsova, E.G.; Ermakov, S.S.; Gas'kov, A.M.; Baburova, P.I.; Sokolova, D.N.; Smirnov, V.M. Three-component working electrode micron-sized Ag particles/TiO<sub>2</sub> layer/Ti: Template electrochemical synthesis and potential use as electrochemical sensor for glutathione detection. *Mater. Res. Express* **2020**, *7*, 035401. [[CrossRef](#)]
43. Li, G.; Cao, H.; Zhang, W.; Ding, X.; Yang, G.; Qiao, Y.; Liu, X.; Jiang, X. Enhanced Osseointegration of Hierarchical Micro/Nanotopographic Titanium Fabricated by Microarc Oxidation and Electrochemical Treatment. *ACS Appl. Mater. Interfaces* **2016**, *8*, 3840–3852. [[CrossRef](#)] [[PubMed](#)]
44. Pei, X.; Ma, L.; Zhang, B.; Sun, J.; Sun, Y.; Fan, Y.; Gou, Z.; Jou, C.; Zhang, X. Creating hierarchical porosity hydroxyapatite scaffolds with osteoinduction by three-dimensional printing and microwave sintering. *Biofabrication* **2017**, *9*, 045008. [[CrossRef](#)]
45. Xu, J.; Chen, X.; Zhang, C.; Liu, Y.; Wang, J.; Deng, F. Improved bioactivity of selective laser melting titanium: Surface modification with micro-/nano-textured hierarchical topography and bone regeneration performance evaluation. *Mater. Sci. Eng. C* **2016**, *68*, 229–240. [[CrossRef](#)] [[PubMed](#)]
46. Zemtsova, E.G.; Orehhov, E.V.; Arbenin, A.Y.; Valiev, R.Z.; Smirnov, V.M. The creation of nanocoatings of various morphology on the basis of titanium dioxide on a titanium matrix for bone implant. *Mater. Phys. Mech.* **2016**, *29*, 138–144.
47. Kar, A.; Raja, K.S.; Misra, M. Electrodeposition of hydroxyapatite onto nanotubular TiO<sub>2</sub> for implant applications. *Surf. Coat. Technol.* **2006**, *201*, 3723–3731. [[CrossRef](#)]
48. Qiu, X.; Wan, P.; Tan, L.; Fan, X.; Yang, K. Preliminary research on a novel bioactive silicon doped calcium phosphate coating on AZ31 magnesium alloy via electrodeposition. *Mater. Sci. Eng. C* **2014**, *36*, 65–76. [[CrossRef](#)] [[PubMed](#)]
49. Eisenbarth, E.; Velten, D.; Schenk-Meuser, K.; Linez, P.; Biehl, V.; Duschner, H.; Hildebrand, H. Interactions between cells and titanium surfaces. *Biomol. Eng.* **2002**, *19*, 243–249. [[CrossRef](#)]
50. Safavi, M.S.; Walsh, F.C.; Surmeneva, M.A.; Surmenev, R.A.; Khalil-Allafi, J. Electrodeposited hydroxyapatite-based biocoatings: Recent progress and future challenges. *Coatings* **2021**, *11*, 110.
51. Lin, W.C.; Chuang, C.C.; Wang, P.T.; Tang, C.M. A comparative study on the direct and pulsed current electrodeposition of cobalt-substituted hydroxyapatite for magnetic resonance imaging application. *Materials* **2019**, *12*, 116. [[CrossRef](#)] [[PubMed](#)]